Hazard assessment modeling and software development of earthquake-triggered landslides in the Sichuan-Yunnan area, China

Xiaoyi Shao[1,2], Siyuan Ma[3,4], Chong Xu[1,2]*

1. National Institute of Natural Hazards, Ministry of Emergency Management of China, Beijing 100085, China

2. Key Laboratory of Compound and Chained Natural Hazards Dynamics, Ministry of Emergency Management of China, Beijing 100085, China

3. Institute of Geology, China Earthquake Administration, Beijing, 100029, China;

4. Key Laboratory of Seismic and Volcanic Hazards, Institute of Geology, China Earthquake Administration, Beijing, 100029, China

*Corresponding to Chong Xu (xc11111111@126.com)

Abstract：To enhance the timeliness and accuracy of spatial prediction of co-seismic landslides, we propose an improved three-stage spatial prediction strategy and developed a corresponding hazard assessment software named Mat.LShazard V1.0. Based on this software, we evaluate the applicability of this improved spatial prediction strategy in six earthquake events that have occurred near the Sichuan Yunnan region, including the Wenchuan, Ludian, Lushan, Jiuzhaigou, Minxian and Yushu earthquakes. The results indicate that in the first stage (immediately after the quake event), except for the 2013 Minxian earthquake, the AUC values of the modelling performance in other five events are above 0.8. Among them, the AUC value of the Wenchuan earthquake is the highest, reaching 0.947. The prediction results in the first stage can meet the requirements of emergency rescue with immediately obtaining the overall predicted information of the possible coseismic landslide locations in the quake-affected area. In the second and third stages, with the improvement of landslide data quality, the prediction ability of the model based on the entire landslide database is gradually improved. Based on the entire landslide database, the AUC value of the six events exceeds 0.9, indicating a very high prediction accuracy. For the second and third stages, the predicted landslide area (Ap) is relatively consistent with the observed landslide area (Ao). However, based on the incomplete landslide data in the meizoseismal area, Ap is much smaller than Ao. When the prediction model based on complete landslide data is built, Ap is nearly identical to Ao. This study provides a new application tool for coseismic landslide disaster prevention and mitigation in different stages of emergency rescue, temporary resettlement, and late reconstruction after a major earthquake.

Keywords: Major earthquake; Earthquake-induced landslide; Hazard assessment; Logistic Regression model; Sichuan-Yunnan area;

1 Introduction

Coseismic landslides are one of the most widespread and destructive hazards triggered by earthquakes in mountainous geological environments (Robinson et al., 2017). The Sichuan-Yunnan region of China has experienced frequent seismic activity due to the characteristics of crustal movement and the action of active faults (Cheng et al., 2020; Xu et al., 2005). Furthermore, due to the unique subtropical monsoon climate with rich and concentrated rainfall, the region is considered an intense coseismic-landslide-prone zone (Cui et al., 2009). Therefore, deep scientific understandings of the spatial distribution of earthquake-induced landslides in this area, followed by near real-time emergency assessment (Cao et al., 2019; Tanyas et al., 2019) and medium and long-term risk assessment (Guzzetti et al., 2005; Lari et al., 2014) can effectively reduce the landslide risk after the earthquake, and also serve for emergency rescue and town planning (Lan et al., 2022).

Evaluation and production of landslide susceptibility mapping can be broadly categorized in three different types, including exploratory analysis based on professional experience, Newmark model based on seismic landslide occurrence mechanism, and the data driven-based machine learning model (Shao and Xu, 2022; Tian et al., 2020). In the application of expert knowledge, this method is heavily influenced by subjective human factors, so human experience error is unavoidable.

The physically-based Newmark model is widely used in seismic landslide hazard assessment of multiple earthquake events, including the 1994 Northridge, California, earthquake (Jibson et al., 2000), the 2008 Wenchuan earthquake (Ma and Xu, 2019a), and the 2017 Jiuzhaigou earthquake (Liu et al., 2017). However, since the simplified Newmark method generalizes calculation process and the input parameters of the evaluation results, the regional evaluation results are not ideal in earthquake emergency assessment (Liu et al., 2017; Ma and Xu, 2019b). In contrast, the data-driven machine learning method is frequently employed and has the widest application potential, such as Information value (Demir et al., 2013), logistic regression (Bai et al., 2015; Dai et al., 2001; Umar et al., 2014), fuzzy logic (Ercanoglu and Temiz, 2011; Kritikos et al., 2015), artificial neural network (Pradhan and Saro, 2010), support vector machine (Xu et al., 2012; Yao et al., 2008), etc. Among them, the LR model is one of the most widely used models in the susceptibility assessment of earthquake-induced landslides by virtue of its simplicity, high efficiency, and high prediction accuracy (Reichenbach et al., 2018; Shao and Xu, 2022).

For a single earthquake event, rapidly identifying the high hazard area of landslides is crucial for understanding the total earthquake impacts (Nowicki Jessee et al., 2018; Tanyas et al., 2019). However, the issue of the data-driven machine learning method is that the training model often needs detailed coseismic landslide data. However, seismic landslide mapping is often a difficult and time-consuming task, hindered by issues relating to the collection and processing of appropriate satellite or aerial images, cloud cover, and the slow speeds associated with manual identification and mapping of large numbers of landslides (Robinson et al., 2017). Consequently, the evaluation result based on data-driven methods lags behind practical emergency response, and thus is unable to serve the short-term disaster prevention and mitigation (He et al., 2021; Nowicki et al., 2014).

To address the issue that the current spatial prediction of coseismic landslides is not timely enough for practical application, Ma et al. (2020) propose a three-stage spatial prediction strategy for seismic landslides, including emergency response, temporary resettlement, and late reconstruction, and use this strategy in the 2013

Lushan earthquake event. In the emergency response stage, the Newmark model is used to carry out rapid emergency hazard mapping in the several hours after the earthquake. However, it should be noted that the Newmark model's prediction results are strongly influenced by the input parameters (Dreyfus et al., 2013), and obtaining relatively reasonable geotechnical parameters for a large area is extremely difficult (Wang et al., 2016; Zhuang et al., 2019). As a result, the accuracy of prediction results based on the Newmark model is relatively low, and it cannot meet the needs of emergency assessment (Ma and Xu, 2019b). At the same time, the three-stage prediction strategy has only been tested in the Lushan earthquake, and its applicability in other seismic events with different magnitudes and structural landform environments is still required to be determined.

In recent years, the near real-time coseismic landslide assessment models have become a powerful tool for fast estimates of ground failure hazards. The core of these models is to incorporate the hazard estimate from seismic events by including the ShakeMap data for each earthquake (available in near real-time from the USGS), combined with environmental factor data, thus allowing the model to be applied in near real-time for future events. For example, Nowicki et al. (2014) combine shaking estimates with proxies for slope, geology, and wetness with 1 km resolution to develop a globally applicable model for near real-time prediction of coseismic landslides based on four landslide inventories. Subsequently, Nowicki Jessee et al. (2018) expand the observational landslide data set which includes 23 landslide inventories and develop a new global empirical model. Tanyas et al. (2019) use 25 earthquake-induced landslides and seven independent thematic variables based on the LR model to establish a global slope unit-based model for the near real-time prediction of earthquake-induced landslides. Allstadt et al. (2018) select the 2016 Mw 7.8 New Zealand earthquake as a test case for evaluating the performance and near-real-time response applicability of three published global earthquake-induced landslide models, and the assessment results show that the global models have great potential in earthquake landslide emergency assessment. Simultaneously, Xu et al. (2019) propose a real probability prediction method of coseismic landslides utilizing the Bayesian probability method and LR model, and establish a new generation of Chinese earthquake-triggered landslide hazard model based on 9 real earthquake-triggered landslide cases. However, the nationwide model's applicability in various earthquake cases with different tectonic and geomorphologic environments needs to be further tested.

In view of the issues encountered during the emergency assessment stage of the three-stage spatial prediction strategy for coseismic landslides, the aim of this study is to propose an improved three-stage spatial prediction strategy and develop a corresponding Hazard assessment software called Mat.LShazard V1.0. Based on this software, we evaluate the applicability of this improved spatial prediction strategy in six earthquake events that have occurred near the Sichuan-Yunnan region with different tectonic and geomorphologic environments which include the 2008 Mw 7.9 Wenchuan earthquake, the 2014 Mw 6.6 Ludian earthquake, the 2013 Mw 6.6 Lushan earthquake, the 2017 Mw 6.5 Jiuzhaigou earthquake, the 2013 Mw 5.9 Minxian earthquake and the 2010 Mw 6.9 Yushu earthquake. The results of this study are expected to provide technical supports for the emergency assessment and mid- and long-term hazard zoning of coseismic Landslides in Sichuan and Yunnan regions.

2 Study area

2.1 Geological setting

The Sichuan-Yunnan region is located on the eastern edge of the Tibetan Plateau. Because of the Sichuan Basin blocking and the impact of fluid movement in the lower crust, tectonic activities in this region are extremely complex (Jiang et al., 2012; Tapponnier et al., 2001; Zhang et al., 2003). Furthermore, due to the intricate tectonic mechanism, various types of active faults are developed, such as the Lancangjiang fault, Jinshajiang fault, Xianshuihe fault, Longmenshan fault, Anninghe fault, Honghe fault, Xiaojiang Fault, and other fault zones, which control the occurrence of strong earthquakes in this area (Cheng et al., 2020; Ren et al., 2022; Xu et al., 2005). The result shows that at least 16 magnitude 7.0 or larger earthquake events have occurred since 1327, including four earthquakes with a magnitude larger than 8.0. As a result, this area has also become the most severely affected region associated with earthquake-induced landslide disasters (Huang and Fan, 2013; Zhao et al., 2021). Since 2008, multiple strong earthquakes have frequently struck this area, which triggered massive coseismic landslides. For example, the 2008 Wenchuan earthquake killed tens of thousands of people, with landslides accounting for 30% of the total loss from the earthquake (Cui et al., 2009). The 2013 Lushan earthquake killed 196 people, with 24 missing, at least 11826 injured and more than 968 seriously injured (Xu et al., 2013). These earthquake events induced a large number of coseismic landslides, which not only seriously threatened the safety of people's lives and property and traffic arteries, but also seriously affected the construction and operation of Sichuan Tibet railway, Yunnan Tibet railway, hydropower resources development and other major national projects.

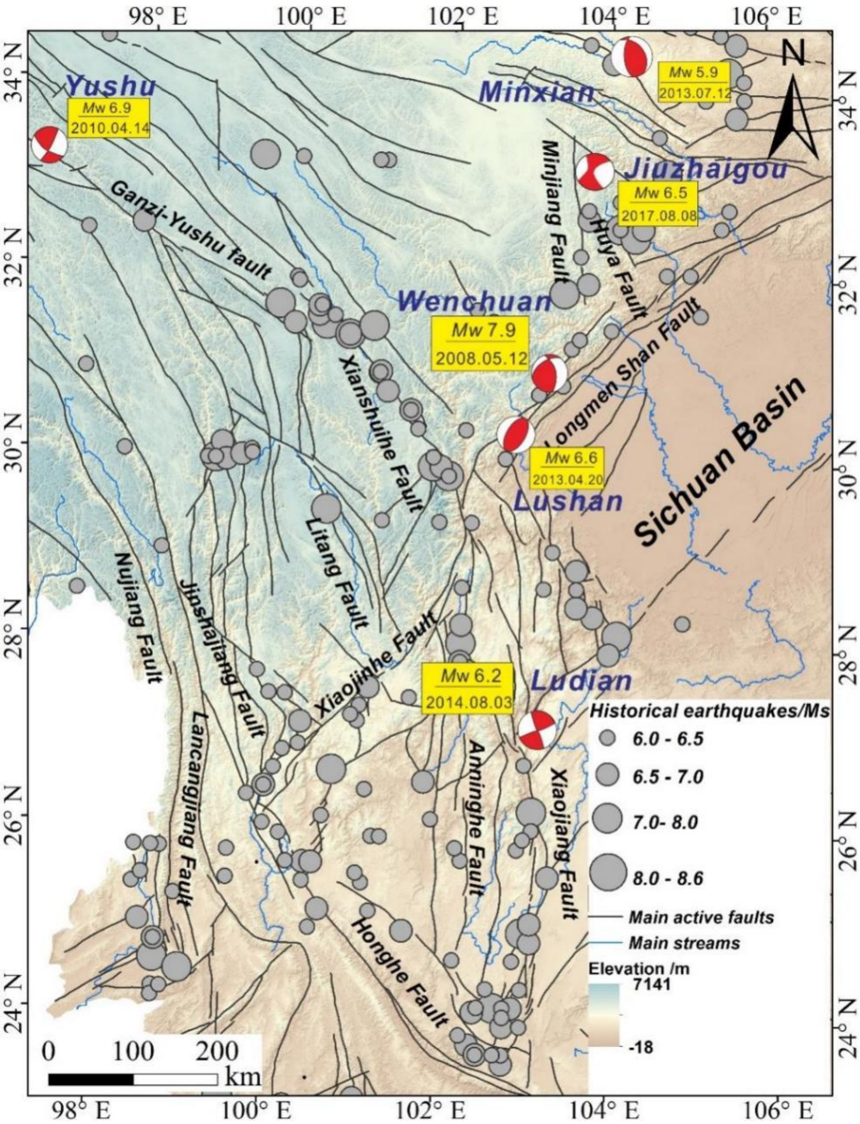

Fig.1 Map showing the topography, earthquakes and tectonic setting of the Sichuan-Yunnan region

2.2 Six landslide inventories

Six landslide-triggered earthquakes have been investigated to test our model (Fig. 2). For all the available inventories, landslides have been mapped as polygons from aerial photographs, satellite images, and also through field surveys including the 2008 Mw 7.9 Wenchuan earthquake (Xu et al., 2014b), the 2014 Mw 6.6 Ludian earthquake (Wu et al., 2020), the 2013 Mw 6.6 Lushan earthquake (Xu et al., 2015), the 2017 Mw 6.5 Jiuzhaigou earthquake (Tian et al., 2019), the 2013 Mw 5.9 Minxian earthquake (Tian et al., 2016; Xu et al., 2014a), the 2010 Mw 6.9 Yushu earthquake (Xu and Xu, 2014). Landslides in these inventories are reported without differentiating landslide types. These landslide inventories have the following characteristics: (1) All landslides are mapped as polygons with clear boundary information; (2) All landslides are visually interpreted based on high-resolution images; (3) All landslides are delineated within the whole earthquake affected area.

The 2008 Mw 7.9 Wenchuan earthquake is the result of sudden dislocation of the Yingxiu Beichuan fault in Longmenshan fault zone (Xu et al., 2009). This earthquake has ruptured two large thrust faults along the Longmenshan thrust belt and produced a 240 km-long surface rupture zone along the Yingxiu-Beichuan fault and a 72 km-long surface rupture zone along the Guanxian-Jiangyou fault. The earthquake has triggered nearly 200 thousand landslides, covering an area of about 311880 km^2.

The Mw 6.6 Lushan earthquake occurred on April 14, 2013, which is another strong earthquake that occurred in the southwest section of the Longmenshan mountain range since the 2008 Wenchuan earthquake. The earthquake triggered more than 22528 landslides, covering an area of about 234.4 km^2.

The Mw5.9 Minxian earthquake on July 12, 2013 occurred within the Lintan-Dangchang fault, located between the East Kunlun fault and the Northern margin of the West Qinling fault (Zheng et al., 2013). The focal depth of this earthquake is 8.2 km. The earthquake triggered more than 6479 landslides, covering an area of about 830.2 km^2.

The seismogenic structure of the Mw 6.6 Ludian earthquake is the NNW-striking Baogunao-Xiaohe fault. The hypocenter is located at a depth of 12 km. The earthquake triggered more than 1024 landslides, covering an area of about 234.4 km^2.

The Mw 6.5 Jiuzhaigou earthquake occurred on 8 August 2017 in Sichuan province, China. The depth of the hypocenter was estimated to be around 9 km. The main seismogenic structure of this earthquake may be a branch of the Tazang fault, or the northern part of the Huya fault. According to the focal mechanism solution, the strike of the seismogenic fault is NW-SE, the dip is SW, and the fault is a left-lateral strike-slip earthquake (Sun et al., 2018). The earthquake triggered about 5986 landslides, and the total area is about 9.6km^2.

The M_W 6. 9 Yushu earthquake occurred near Qinghai province on 4 April 2010. The hypocenter is located at a depth of 17 km within the Ganzi–Yushu strike-slip fault(Chen et al., 2010). The earthquake produced a surface fracture zone with a strike of about 300° and a length of 65 km. The surface rupture zone is characterized by left-lateral strike-slip fault. The surface rupture zone is composed of a series of extrusion bulge and tension fractures (Chen et al., 2010). The earthquake triggered almost 2036 landslides with an area of about 1455.3 km^2.

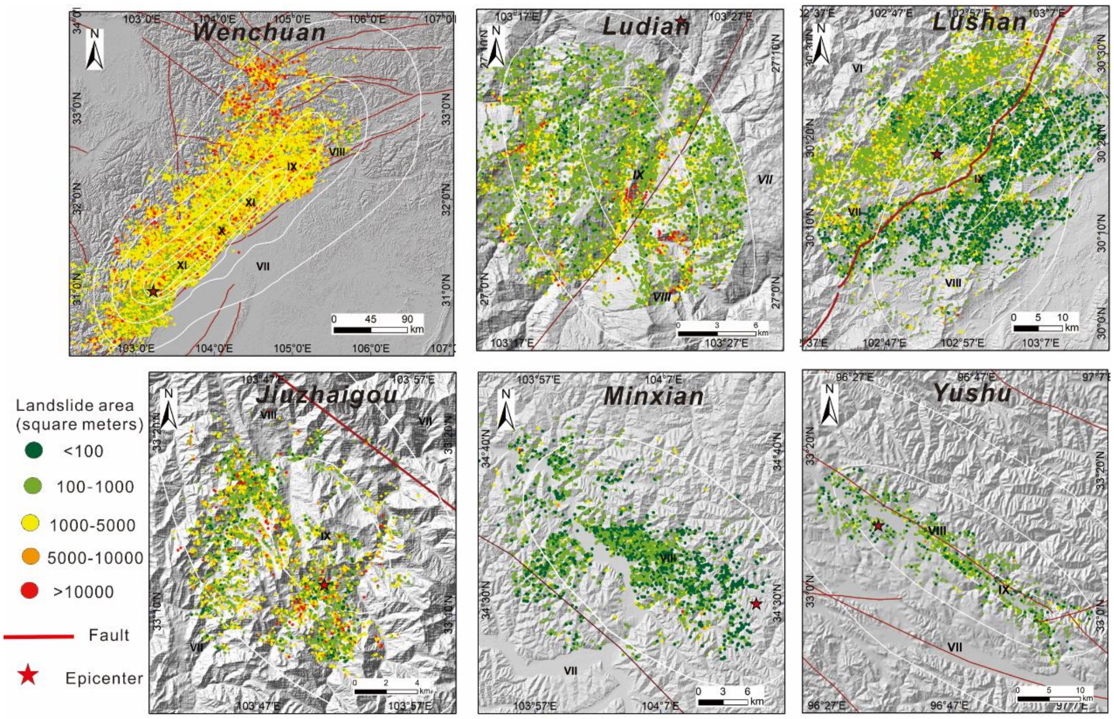

Fig.2 Six earthquake-induced landslide inventories used in this study. White lines show spatial distribution of the seismic intensity, provided by the China Earthquake Networks Center(CENC)

3 Data and Software

3.1 Data sources

Earthquake-induced landslides are mainly controlled by earthquakes, topography, geology, hydrology and other factors (Nowicki Jessee et al., 2018; Reichenbach et al., 2018). In this study, 11 influencing factors are selected to establish the LR model for the second and third stages, including elevation, hillslope gradient, slope aspect, topographic relief, curvature, topographic wetness index (TWI), vegetation coverage percentage, distance from fault, lithology, annual average precipitation and seismic intensity.

The elevation data are acquired from SRTM DEM, and its projection resolution is 30m (Jarvis et al., 2008). The hillslope gradient, slope aspect and curvature are extracted using this elevation data and ArcGIS software. Topographic relief and TWI are also computed using GRASS GIS based on the elevation data. The slope position is calculated by the LandFacetCorridor program (Jenness et al., 2013). We consider a global data set that represents the maximum green vegetation fraction (0–100%) to characterize the vegetation coverage of the land area and the water bodies; the vegetation coverage is assigned as -1 (Tateishi, 2010). The distribution of active fault data are acquired from National seismicity fault database (Xu et al., 2016). The distances from the centroid of the grid cells to the nearest fault are calculated using ArcGIS. The distribution of seismic intensity for every seismic event is provided by China Earthquake Networks Center (https://www.cenc.ac.cn/cenc/zgdztw/index.html), and then the raster format for the seismic intensity is obtained by the Kriging interpolation.

The stratigraphic data are from the 1:2,500,000 geological map published by China Geological Survey (http://dcc.cgs.gov.cn/). We divide the lithology into 12 categories according to the stratigraphic ages, which are Quaternary (Q), Tertiary (R), Cretaceous (K), Jurassic (J), Triassic (Tr), Permian (P), Carboniferous (C), Devonian (D), Silurian (S), Ordovician (O), Cambrian (∈) and Precambrian (Pre∈). The annual average rainfall data are obtained from 1 km spatial resolution climate surfaces for global land areas of WorldClim 2 dataset(Fick and Hijmans, 2017). Finally, the spatial distribution of the 11 influencing factors is converted into a raster format with a grid cell size of 30 m.

3.2 Mat.LShazard V1.0 Software description

3.21 The computational framework

A number of tools for landslide hazard assessment are already available in current studies, such as GIS-based LSAT toolbox (Polat, 2021), LAND-SE implemented in R (Rossi and Reichenbach, 2016), r.landslide module based on GRASSGIS (Bragagnolo et al., 2020), GeoFIS (Osna et al., 2014), and LSAT PM v1.0 (Torizin et al., 2022), providing great convenience for us to conduct the regional landslide susceptibility assessment. However, to our knowledge, there currently no specialized software for coseismic landslide hazard assessment, particularly in the various needs of different stages after a major earthquake.

Based on MATLAB, we develop an earthquake-induced hazard assessment software named Mat.LShazard V1.0. This section describes the computational framework and operation of the software. A flowchart describing the module is presented in Fig.3. Data input, model training, and model validation are the three main components of the software. Landslide data and the influencing factors of the study area are used for the input data. These data are in TIFF grid layer format. We employ the LR model for model training. We train the LR model using the aforementioned input data, and then produce the seismic landslide hazard maps. Finally, in order to assess and confirm the accuracy of the model's prediction outputs, three indexes are chosen for the verification of the receiver operating characteristics curve (ROC), the confusion matrix and the predicted landslide area (Ap).

It is important to note that Mat.LShazard V1.0 is not the same as the traditional landslide susceptibility software. The goal of this software is to meet the needs of various stages following a major earthquake. As a result, for different stages, we calculate seismic landslide hazard assessment results based on different LR models. For the emergency rescue stage I (immediately after the quake event), we select the new generation of Chinese earthquake-triggered landslide hazard model, which is established by 9 earthquake cases, including 306435 real earthquake landslide records and 13 influencing factors with a 100m resolution (Xu et al., 2019). A total of 13 influencing factors are selected for model conformation, including elevation, topographic relief, hillslope gradient, slope aspect, slope curvature, slope position, topographic wetness index, land-over type, vegetation coverage percentage, distance to the fault, lithology, average annual precipitation and seismic intensity. More detailed theory and calculation procedures can be found in supplementary materials. In the absence of seismic landslide data, this model can produce seismic landslide hazard distribution map for stage I with only the seismic intensity map.

For temporary resettlement stage II (hours to a few days (e.g., Planet)), remote sensing images can be gradually obtained following the earthquake. Based on visual interpretation or automatic identification, we can obtain the seismic landslide distribution map of the meizoseismal area, which can be used as the preliminary results of this event. We choose the similar influencing factors as the model's input for the second and third stages, so that we can easily compare the regression coefficient changes of different influencing factors in different stages and thus explain the relationship between each influencing factor and the earthquake-induced landslide occurrence. Combined with the above influencing factors with a 30m resolution and incomplete landslide data, we can establish a new LR model and provide the seismic landslide hazard distribution map for stage II.

For the late reconstruction stage III (few days to weeks (e.g., Planet, Sentinel 2, Landsat 8/9)), a large number of remote sensing images collected before and after the earthquake in the quake-affected area can be obtained, which can effectively cover the entire earthquake area, realizing the establishment of a comprehensive earthquake-induced landslide inventory. In stage III, we are faced with not only the problem of identification of coseismic landslide, but also the weakened slope caused by the quake. As a result, it is critical to locate the landslide that is stable during the earthquake but unstable for a period of time after the earthquake. At this stage, we combine the complete landslide data and influencing factor data with a 30m resolution to train and update the LR model, and provide the seismic landslide hazard map for stage III. Therefore, the results obtained in stage III will definitely be more objective than those obtained in the stage II, because the training samples used in the model in this stage are more abundant and objective.

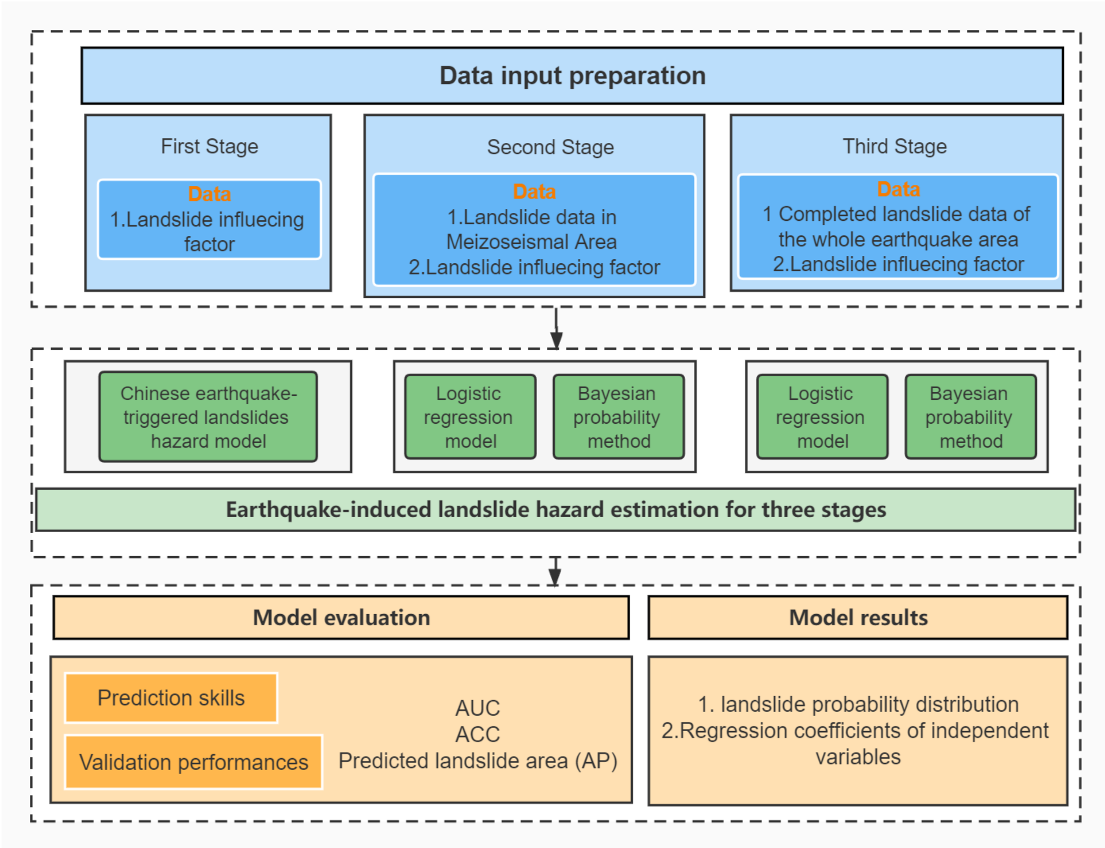

Fig.3 Logical schema of the Mat.LShazard V1.0 software for earthquake-induced hazard assessment

3.22 Logistic Regression model

Logistic regression model (LR) is a statistical model that predicts the probability of one event taking place by having the log-odds (the logarithm of the odds) for the event be a linear combination of one or more independent variables ("predictors") (Dai and Lee, 2002; Merghadi et al., 2020; Tolles and Meurer, 2016). It is a nonlinear multivariate statistical model that has been widely used in landslide hazard modeling by virtue of its simplicity, high efficiency, and high prediction accuracy (Allstadt et al., 2018; Broeckx et al., 2018; Lin et al., 2017; Massey et al., 2018; Reichenbach et al., 2018). It is also the preferred method for establishing the near-real-time prediction model of earthquake-induced landslides (Nowicki Jessee et al., 2018; Tanyas et al., 2019; Xu et al., 2019). LR model converts dependent variables into binary logic variables that occur (recorded as 1) and do not occur (recorded as 0). The relationship between landslide occurrence probability and impact factors can be expressed as:

$$Z = \beta_0 + \beta_1\chi_1 + \beta_2\chi_2 + \beta_3\chi_3 \dots \beta_i\chi_i \quad (1)$$

$$P = 1/(1 + e^{-z}) \quad (2)$$

Where P represents the probability of landslide occurrence, ranging from 0 to 1. Z represents the sum of linear weight values after variable superposition. χ_i denotes each impact factor, and β_i is the corresponding regression coefficient.

3.22 Bayesian probability method

The aim of this study is to develop a probability estimator for predicting the areal extent of landslides. In other words, we correlate the resulting probability with spatial extent (e.g., areas labeled 5% probability of landsliding contain about 5% landslides by area) (Nowicki Jessee et al., 2018; Shao et al., 2020b). As a result, we generate sample points randomly in the study area. The points within the landslide area are sliding samples, while the others are not; such setting ensures that the ratio of sliding to non-sliding is equivalent to the probability of coseismic landslides occurring in the study area (Shao et al., 2020b). The coseismic landslide probability (Pcols) in the region is simply defined as the ratio of the area of all landslides to the total area of the region based on Bayesian theory:

$$P_{cols} = \frac{A_l}{A_s} \times 100\% \quad (3)$$

where A_l is the total area of all coseismic landslides and As is the area of the entire study area.

Based on the above Bayesian probability method and the corresponding landslide surface data, the corresponding landslide sample points and non-landslide sample points can be randomly generated; thus, the predictive model can be constructed.

3.23 Model validation

In this study, three indexes including the receiver operating characteristics (ROC) curve, the confusion matrix and the predicted landslide area (Ap) are used to evaluate our results. First, we assess the modelling performance by checking the variation in AUC value (varying between 0.5 for a random classification model and 1 for the best performance), which is a metric referring to the area under the ROC Curve (Brenning, 2005; Swets, 1988). Second, we use the confusion matrix for the performance evaluations of the prediction results. The confusion matrix consists of four basic characteristics (numbers) that are used to define the measurement metrics of the classifier, which are TP (True Positive), TN (True Negative), FP (False Positive) and FN (False Negative) (Fawcett, 2006), respectively. One of the most commonly employed metrics for classification is accuracy. The accuracy of a model through a confusion matrix is calculated using the formula expressed as:

$$\mathrm{Accuracy} = {TP + TN}/{TN + FP + FN + TP} \quad (4)$$

Otherwise, in order to evaluate the model prediction performance, we compute the predicted landslide area (Ap) as a metric to summarize the total hazard estimated by a given model for a given earthquake with a single number. The probability value of each grid multiplied by the grid area represents the predicted landslide area in each grid. The predicted landslide area in the study area can be obtained by all grids superposition (Allstadt et al., 2018; Shao et al., 2020b). The predicted landslide area (Ap) is computed by equation 5 (Allstadt et al., 2018; Shao et al., 2020b).

$$\mathrm{A_p} = \sum_{\mathrm{i=1}}^{\mathrm{m}} \sum_{\mathrm{j=1}}^{\mathrm{n}} \mathrm{p_{i,j}} \mathrm{A} \quad (5)$$

in which $\mathrm{p_{i,j}}$ is the probability of a landslide at pixel i and j, m is the number of rows, n is the number of columns, and A is the pixel/cell area (constant).

4 Results and analysis

4.1 First Stage

The landslide hazard estimate of six earthquake events in the first stage (immediately after the event) is obtained using the Chinese earthquake-triggered landslide hazard model (Xu et al., 2019). The predicted results in our software can be processed at the first stage by entering the seismic intensity maps of six cases produced by CENC. Fig.4 shows the predicted probability distribution for six earthquake events in the first stage. Overall, the Chinese earthquake-triggered landslide hazard model has different forecasting abilities for different earthquake events. For the Wenchuan earthquake, the prediction results in this stage are reliable.

The regions with high hazard are primarily found in intensity X and XI, and the distribution of actual landslides also reveals that nearly 80% of the landslides are concentrated in the northeast area with intensity X and XI. In addition, for the 2013 Lushan earthquake and the 2017 Jiuzhaigou earthquake, most of the actual landslides are basically located in high-hazard areas. Especially for the Lushan earthquake, the prediction results can better forecast the northwest region located in the epicenter region, which corresponds to the landslide-concentrated area. For the 2010 Yushu earthquake, the high-hazard area is located in the southeast region with intensity VII and the whole region with intensity IX. The actual coseismic landslides of the Yushu earthquake are primarily distributed in regions with intensity IX, indicating that with the exception of the overestimated southeast region with intensity VII, the remaining area can accurately predict the potential high hazard areas. However, the prediction results of the 2013 Minxian earthquake are barely satisfactory. According to Fig.4e, the high-hazard prediction areas are primarily concentrated in the northwest region with intensity VII and the southwest region with intensity VIII. However, according to the actual distribution of landslides, the most landslides triggered by this earthquake are located in the central region with intensity VIII. Namely, the prediction results do not accurately predict the actual landslide distribution, and the majority of coseismic landslides occur in low-hazard prediction areas.

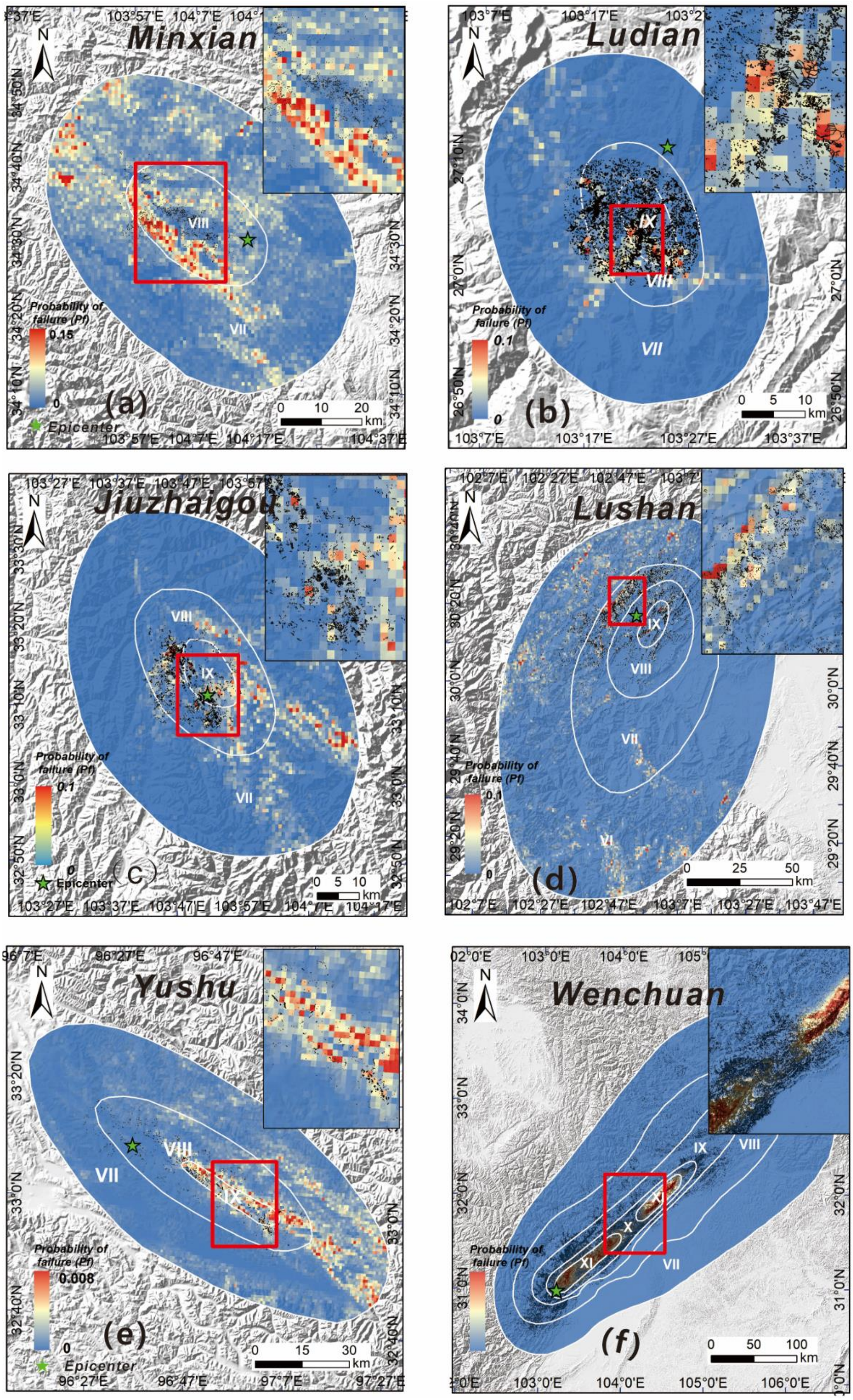

Fig.4 Maps showing predicted landslide probability distribution for six earthquake events in the first stage; (a) the 2013 Mw 5.9 Minxian earthquake; (b) the 2014 Mw 6.6 Ludian earthquake; (c)

the 2017 Mw 6.5 Jiuzhaigou earthquake; (d) the 2013 Mw 6.6 Lushan earthquake; (e) the 2010 Mw 6.9 Yushu earthquake; (f) the 2008 Mw 7.9 Wenchuan earthquake.

We compare the predicted landslide area (Ap) in the first stage with the actual landslide area. Fig.5 shows that the slope of the fitting curve between the predicted and actual areas of the six earthquakes is close to one. The Ap for the Yushu, Lushan, and Wenchuan earthquakes are on the high side, with an error range of 50%-78%. On the other hand, the Ap of Minxian, Ludian and Jiuzhaigou earthquake are on the low side, with an error range of 17%-30%. In general, the prediction results meet the requirements of emergency rescue with quickly obtaining the predicted information of the possible coseismic landslide locations in the whole quake-affected area.

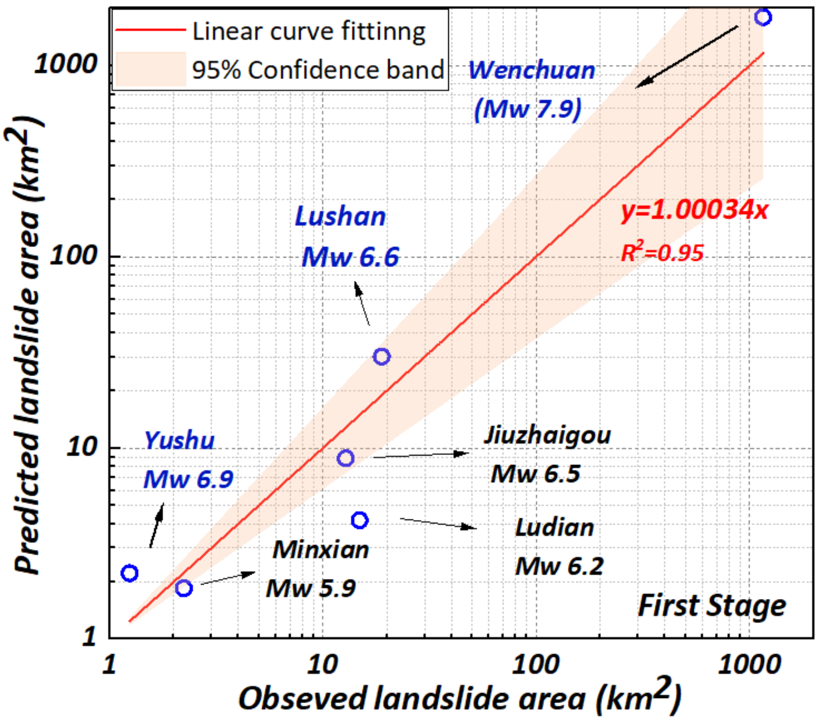

Fig.5 Relationships between the observed landslide area (Ao) and the predicted landslide area (Ap) for six earthquake events in the first stage.

4.2 Second and Third Stages

As mentioned in section 3.21, for the landslide hazard prediction of the second and third stages, we train the evaluation model of these two stages using landslide data from the meizoseismal area and the whole quake-affected area respectively. To reduce the stochastic effects of data sampling, we calculate the LR model by randomly selecting the training samples by considering the uncertainty of the samples (Shao et al., 2020b; Tanyas et al., 2019). We choose 70% of all samples at random and independently repeated 50 times to construct the LR model. All the predicted models for 6 earthquake cases are performed 50 times, yielding 50 predicted pictures of potential landslides in the study area for each event.

Fig.6 shows the mean predicted probability distribution of six events in the second stage (hours to a few days (e.g., Planet)). The majority of the high-hazard areas of six earthquakes are located in high-intensity areas. For example, the high-hazard areas of the Ludian earthquake are concentrated in the meizoseismal area, which is essentially consistent with the actual landslide distribution. However, in the southwest region where landslides are well developed beyond the meizoseismal area with intensity VIII, the landslide density is high, but the predict probability is quite low. Similar phenomena have been observed in the Jiuzhaigou and Lushan earthquakes. The above phenomenon is less obvious in other three earthquake events including the Minxian, Wenchuan, and Yushu earthquakes. For instance, the seismogenic fault of the Yushu earthquake is a left-lateral strike-slip fault, and thus the majority of the coseismic landslides are basically distributed along both sides of the seismogenic fault. The high-hazard areas of the Yushu earthquake are distributed in the meizoseismal area on both sides of the seismogenic fault, and these areas essentially correspond to the main development areas of seismic landslides.

To obtain the prediction probability distribution map of the third stage, we use all available landslide data from the entire earthquake-affected region (few days to weeks (e.g., Planet, Sentinel 2, Landsat 8 or 9)). Based on the same method, 70% of all samples are used for modeling, and then 50 model results are generated by repeating 50 experiments. Fig.7 shows the mean probability distribution of six events in the third stage. Compared to the second stage, the predicted results in the third one are more consistent with the actual landslide distribution. The majority of actual landslides are basically distributed in areas with high hazard , indicating that the evaluation model has high prediction ability at this stage. Particularly for the Ludian, Jiuzhaigou and

Lushan earthquakes, the assessment results can better predict the actual landslide distribution in all earthquake affected areas.

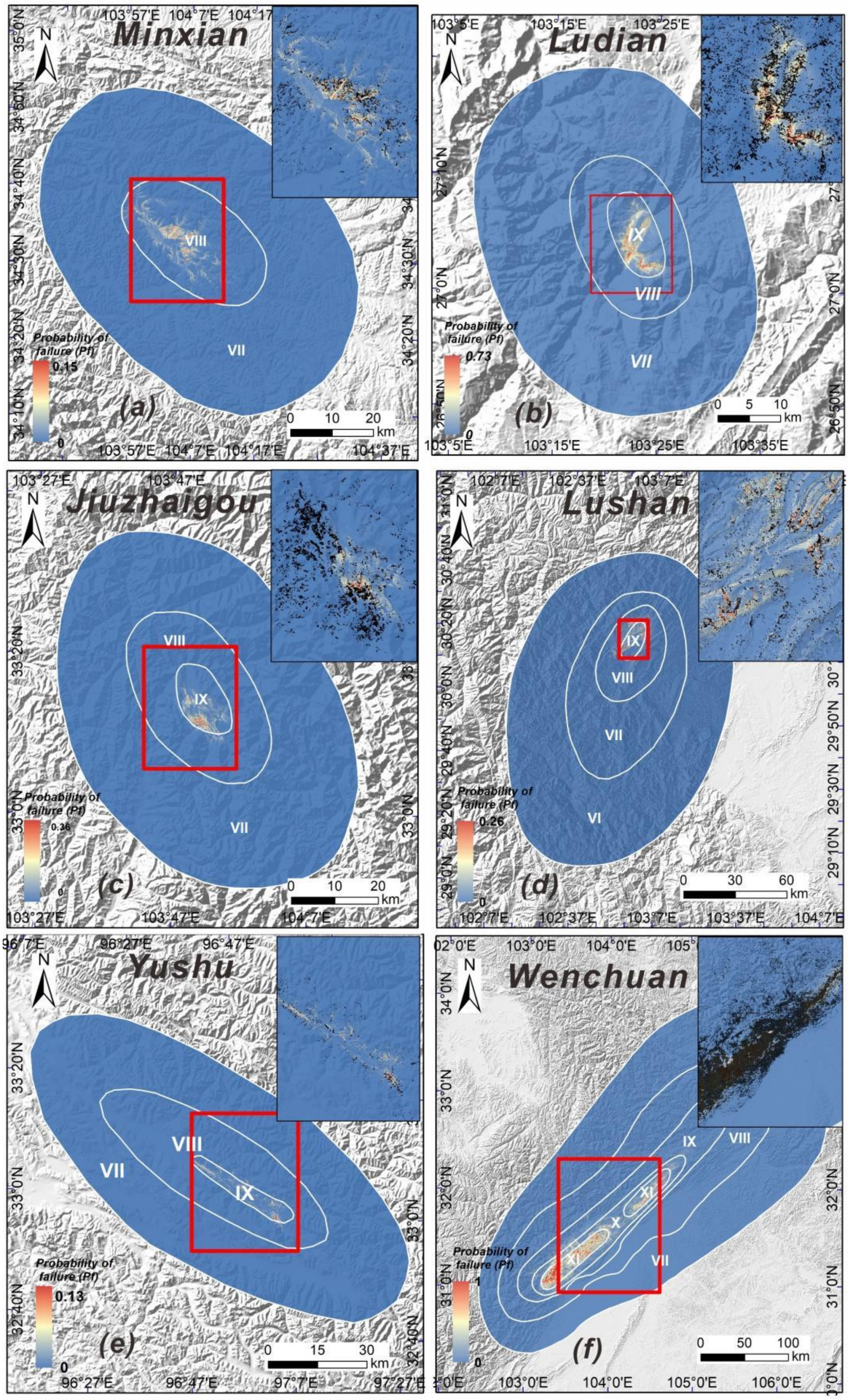

Fig.6 Maps showing predicted landslide probability distribution for six earthquake events in the second stage; (a) the 2013 Mw 5.9 Minxian earthquake; (b) the 2014 Mw 6.6 Ludian earthquake;

443 (c) the 2017 Mw 6.5 Jiuzhaigou earthquake; (d) the 2013 Mw 6.6 Lushan earthquake; (e) the

444 2010 Mw 6.9 Yushu earthquake; (f) the 2008 Mw 7.9 Wenchuan earthquake;

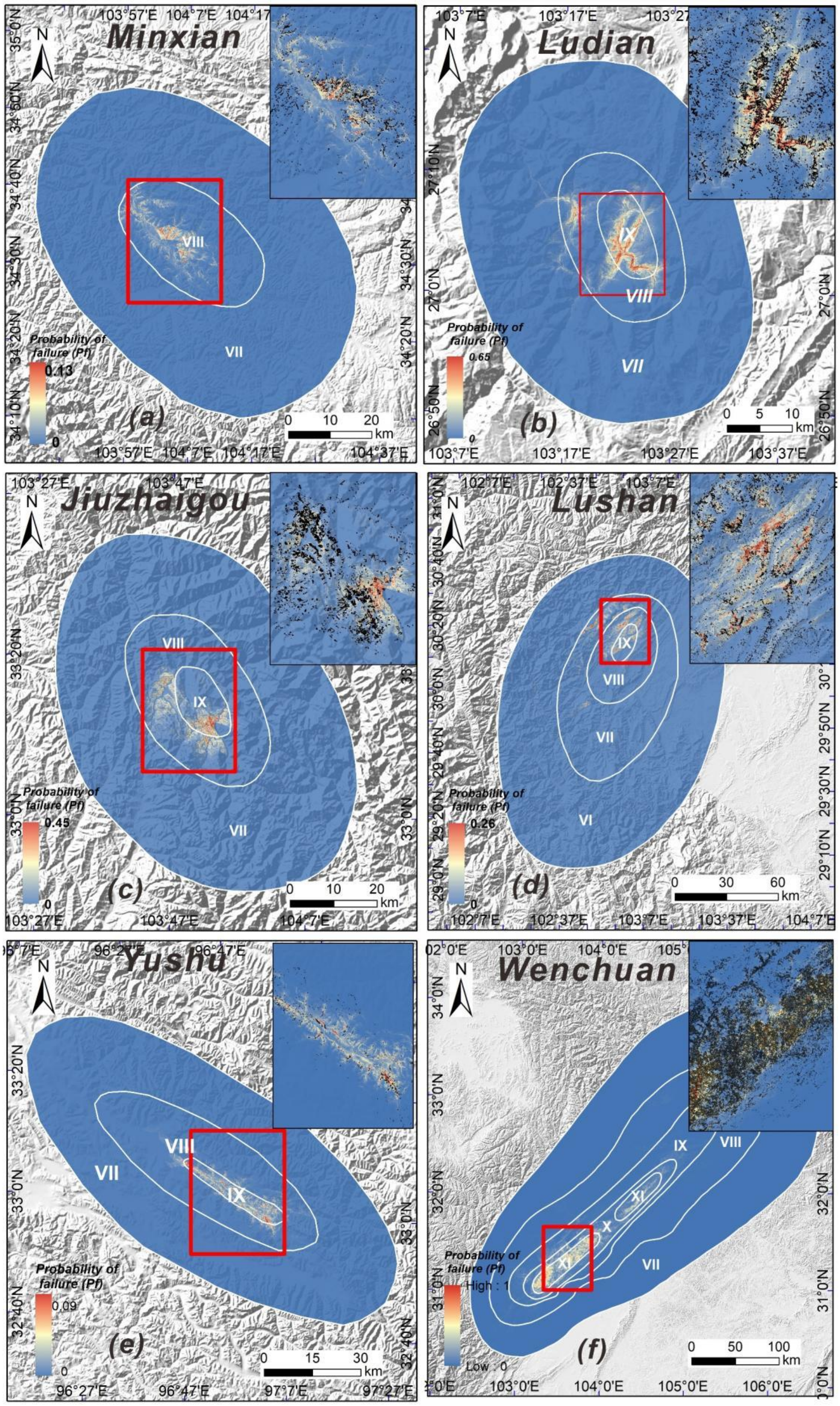

445

Fig.7 Maps showing predicted landslide probability distribution for six earthquake events in the third stage; (a) the 2013 Mw 5.9 Minxian earthquake; (b) the 2014 Mw 6.6 Ludian earthquake; (c) the 2017 Mw 6.5 Jiuzhaigou earthquake; (d) the 2013 Mw 6.6 Lushan earthquake; (e) the 2010 Mw 6.9 Yushu earthquake; (f) the 2008 Mw 7.9 Wenchuan earthquake;

Fig.8 shows the relationships between the observed landslide area (Ao) and the predicted landslide area (Ap) for six earthquake events in the second and third stages. The results show that whether in the second or third stage, Ap is in good agreement with Ao. In the second and third stages, the slope of the fitting curves of the two stages are 0.86 and 1.01 respectively. In addition, we can observe that in the second stage, the Ap of the six earthquakes are generally lower than the corresponding Ao, and the overall error is between 9% and 74%. Among them, the prediction error of the Wenchuan earthquake is the lowest (9%), and the error of the Jiuzhaigou earthquake is the highest, reaching 74%. For the six cases in the third stage, Ap is basically consistent with Ao, and the error range is about 1%, showing high performance of LR model in this stage.

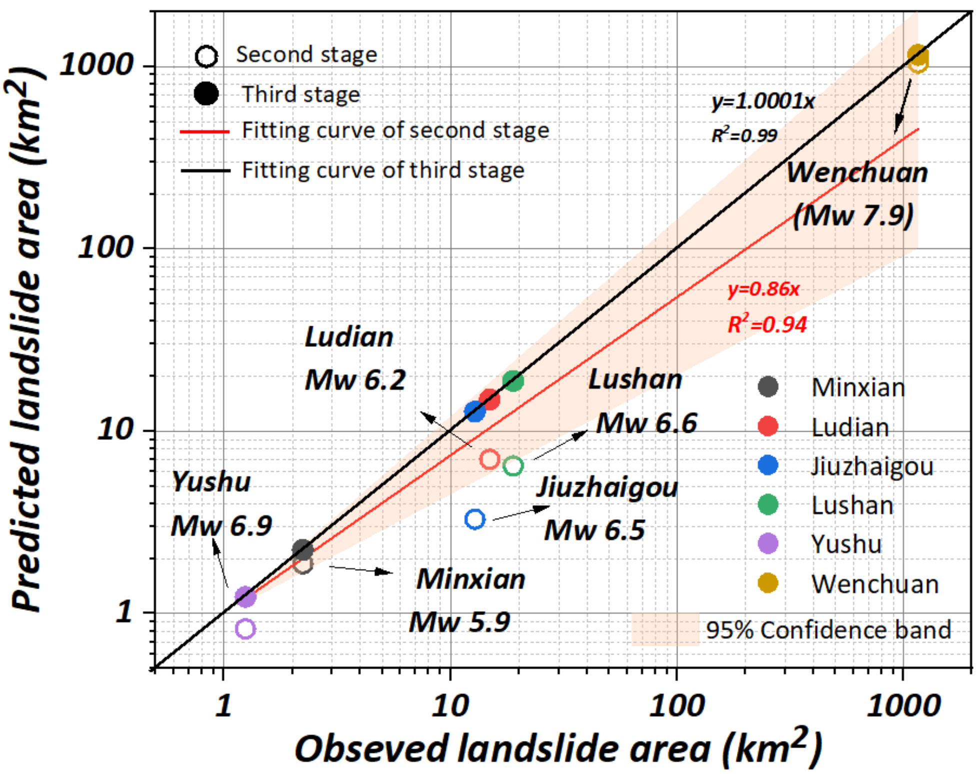

Fig.8 Relationships between the observed landslide area (Ao) and the predicted landslide area (Ap) for six earthquake events in the second and third stages; The hollow and filled circles represent the predicted landslide area for the second and third stages, respectively. The red and black lines represent the fitting curves of the second and third stages, respectively.

Fig.9 shows the distribution of regression coefficients of various influencing factors in the second and third stages. For continuous variables, if the regression coefficient is positive, with the increase of the independent variable, the probability of landslide is larger (Nowicki Jessee et al., 2018; Shao et al., 2020a). According to the regression coefficient, we can explain the relationship between each influencing factor and the corresponding landslide occurrence. We choose four independent variables that have large impact on landslide occurrence, namely, topographic relief, hillslope gradient, seismic intensity, and distance to seismogenic fault. The results show that regression coefficient of seismic intensity is the largest in all seismic events, followed by hillslope gradient, indicating that the seismic factor and hillslope gradient are the main factors controlling the occurrence of seismic landslides. The distance to fault is another important factor that controls the occurrence of seismic Landslides. The regression coefficient of this variable is negative, implying that it has a negative effect on the occurrence of seismic landslides (i.e., the farther away from the seismogenic fault, the less likely the occurrence of seismic landslides). Furthermore, with the exception of the 2010 Yushu earthquake, the regression coefficients of topographic relief in the other five earthquake events are all positive, indicating that topographic relief in other five earthquake events plays an essential role in the occurrence of seismic landslides. Fig.S1 shows LR regression coefficients of all continuous independent variables of six earthquake events in different stages.

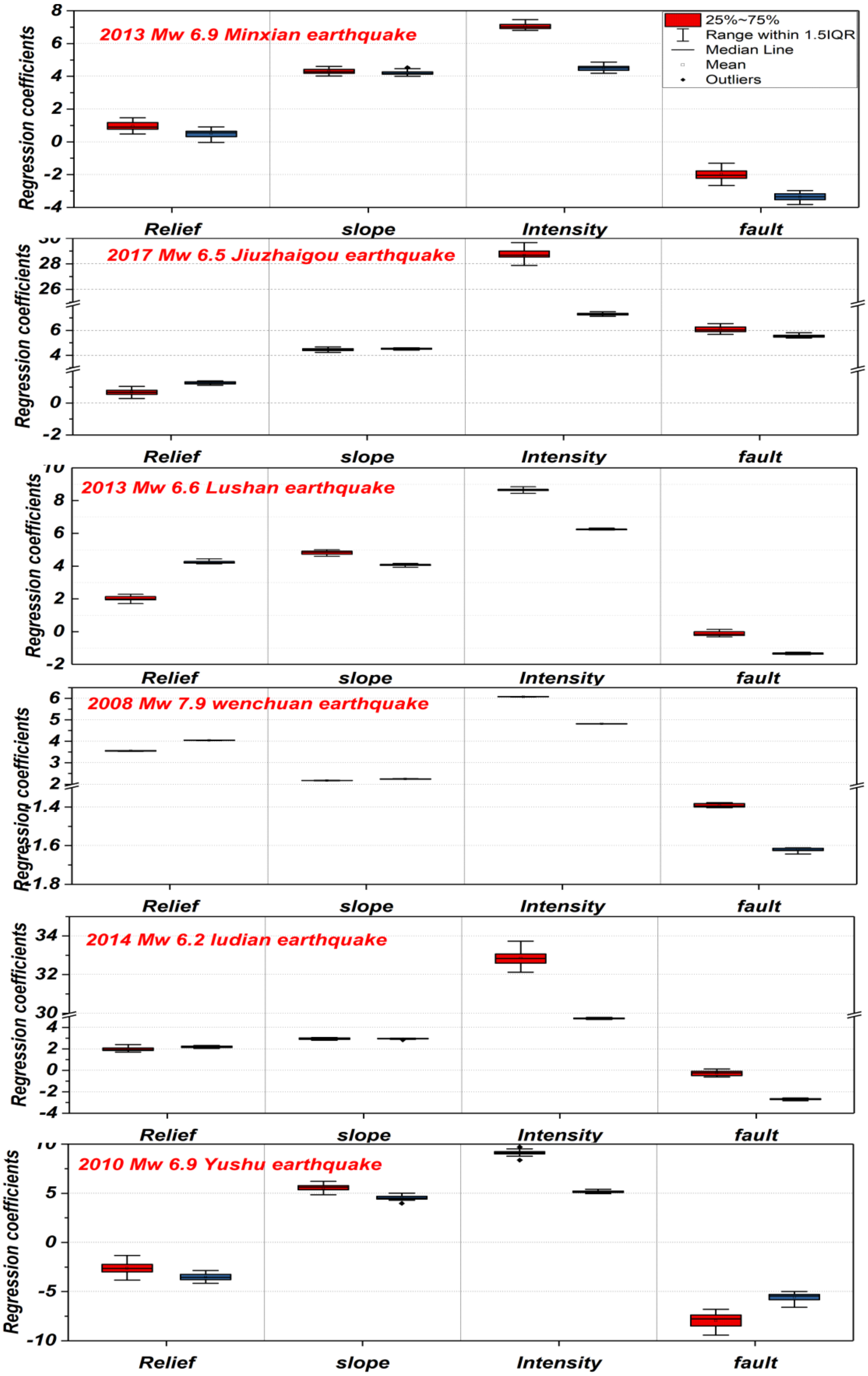

487

488 Fig.9 Regression coefficients of independent variables at different evaluation stages; The red box
489 chart represents the regression coefficients of the independent variables in the second stage, and
490 the blue chart represents the regression coefficients of the independent variables in the third
491 stage

4.3 Quantitative analysis

In order to quantitatively analyze the model results of the six earthquakes at different stages, three indexes including the receiver operating characteristics curve (ROC), the confusion matrix, and the predicted landslide area (Ap) are used to evaluate our model results. Fig.10 and Table S1 show the predicted landslide area for six earthquake events in different stages. The results reveal that the Ap of the three events including the Minxian, Ludian, and Jiuzhaigou earthquakes in the first stage is much lower than the corresponding Ao, whereas the Ap of the Lushan, Yushu, and Wenchuan earthquakes is significantly greater. Furthermore, based on incomplete landslide data in the meizoseismal area, Ap is much smaller than Ao. However, when the prediction model of the third stage based on complete landslide data is built, Ap is nearly identical to Ao.

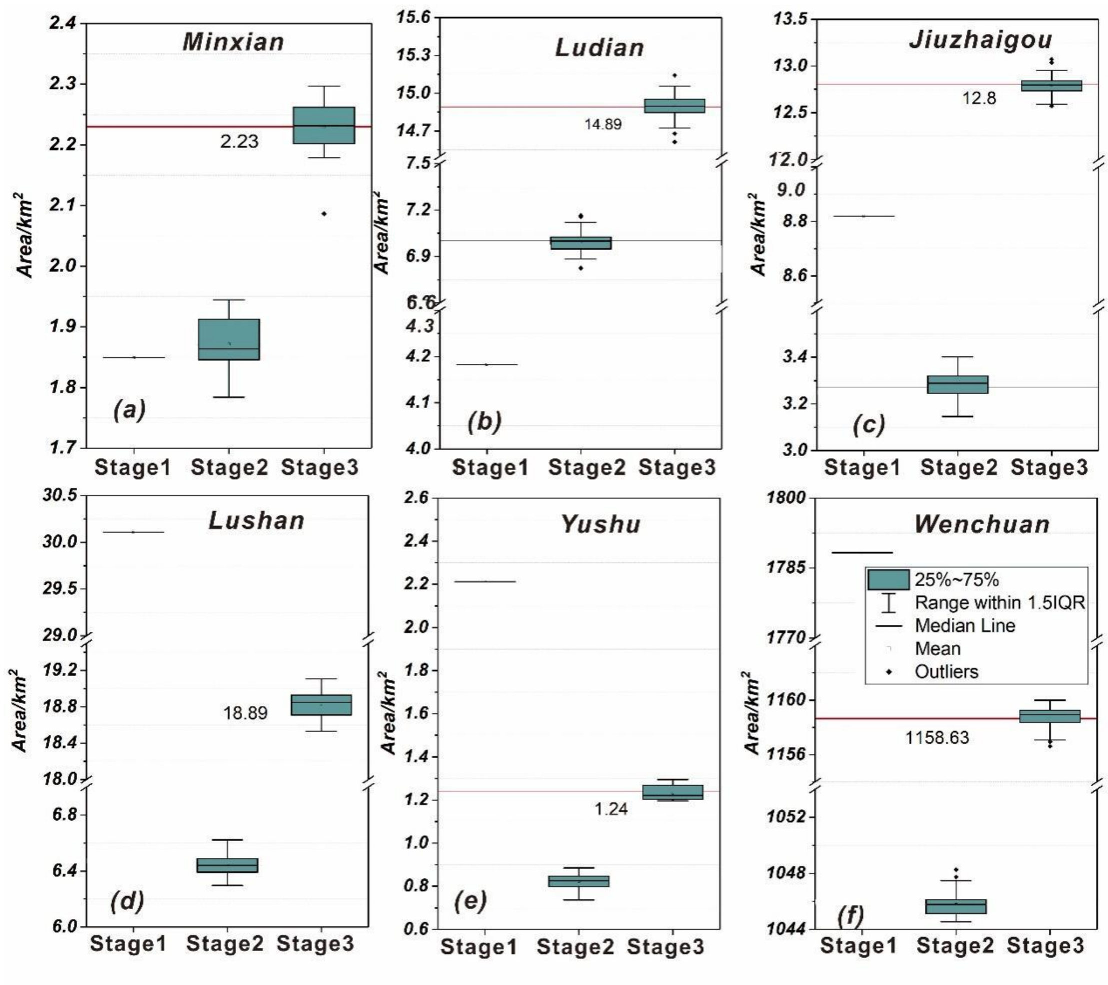

Fig.10 Predicted landslide area for six earthquake events in different evaluation stages. The

horizontal line represents the total area of landslides triggered by this earthquake

In this study, we randomly select 70% of the total samples for model training, and the remaining 30% are used for modeling validation. Fig.11 and Table S2 show the distribution of AUC values based on validation samples for six earthquake events in different stages. The results show that except for the Ludian earthquake, the prediction accuracy of the model outputs for other five earthquake events exhibits an upward trend. In the first stage, the AUC value of the modelling performance of the Wenchuan earthquake is the highest, reaching 0.947, while the AUC value of the Minxian earthquake is the lowest, only 0.57. Additionally, the AUC values of other four earthquakes range from 0.8 to 0.85. In the second and third stages, we can observe that as landslide data quality is continuously improved, the prediction accuracy of the model based on the entire landslide database is gradually increased. Based on the entire landslide database, the AUC value of six events exceeds 0.9, indicating a very high prediction accuracy.

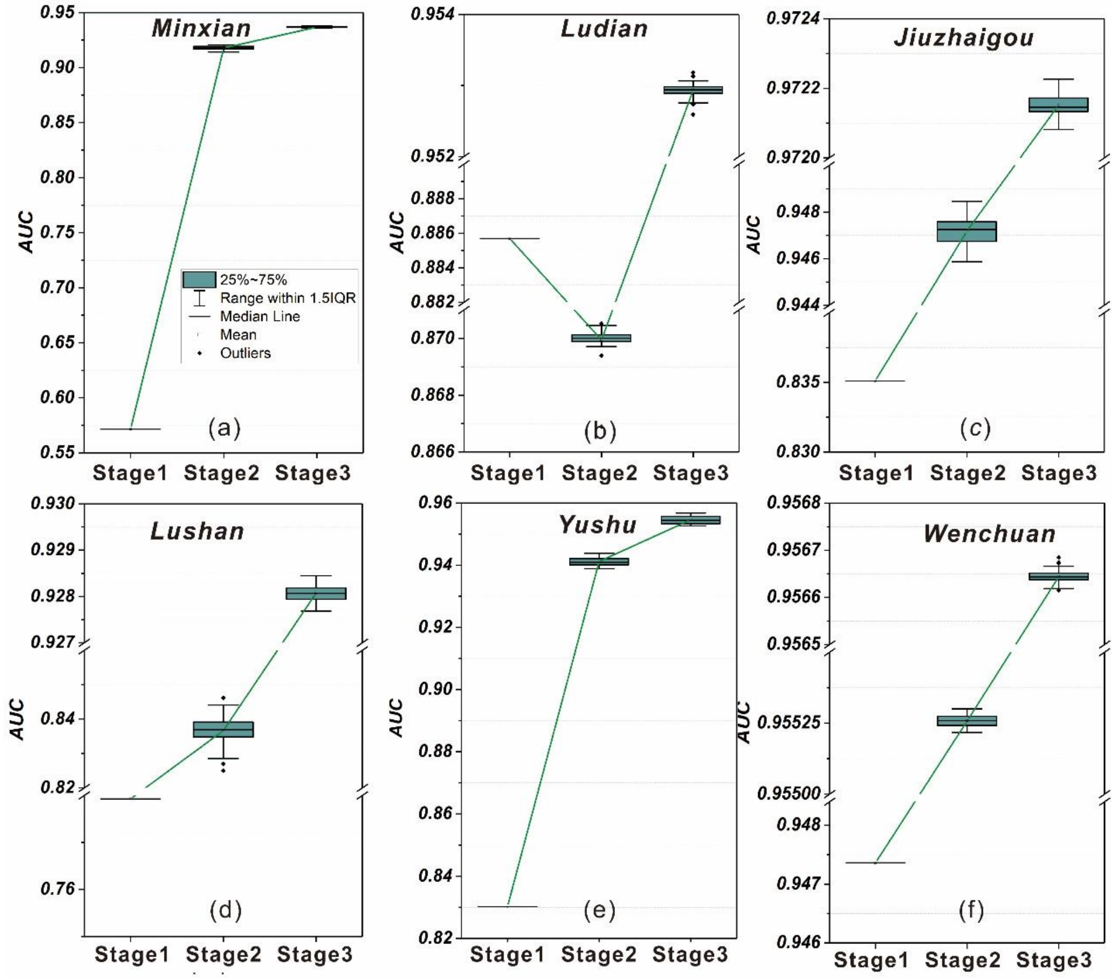

Fig.11 Distribution of AUC values for the six earthquake events in different evaluation stages.

Fig. 12 and Table S3 show the calculated model accuracy using actual landslide data from the six seismic events at different stages. The accuracy of the model fluctuates from 58% to 78% at the first stage, indicating that the model's applicability in different seismic events changes. In the second stage, with the exception of the Wenchuan earthquake, the accuracy of other earthquake events is less than 80%. In the third stage, the model accuracy of all seismic events exceeds 80%, with the Jiuzhaigou event reaching 91%.

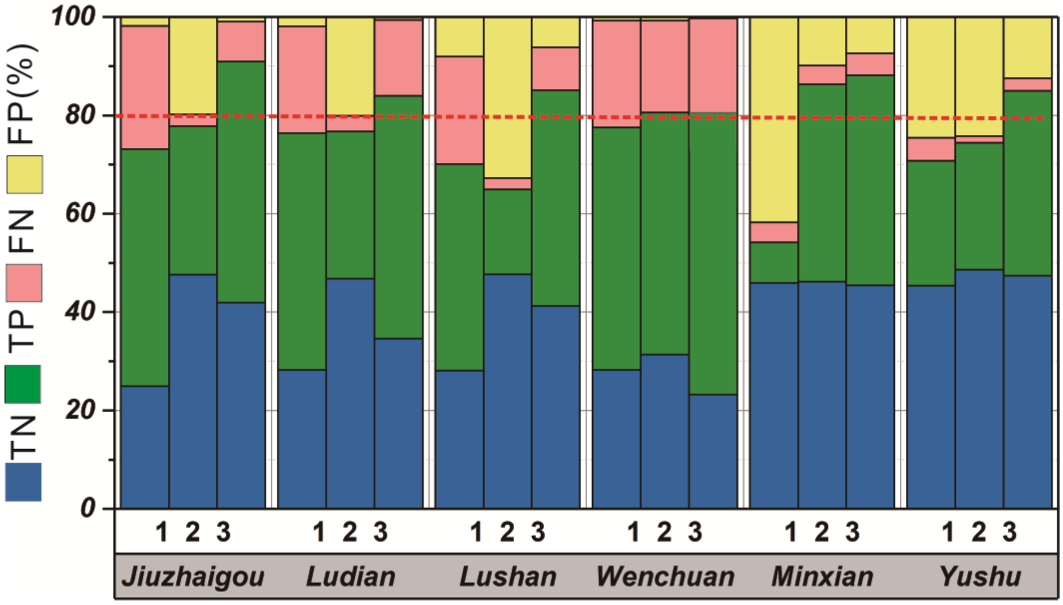

Fig.12 Results of models validated by the six earthquake inventories. TN: True Negative; TP: True Positive; FN: False Negative; FP: False Positive. The accuracy (ACC) of the models represented graphically by the sum of the two lower bars.

5 Discussion

Time is of the essence in the emergency response stage I. Rapid evaluation of earthquake-induced landslides can quickly determine the high-hazard areas of seismic landslides and provide a basis for optimizing emergency deployment. Although the Newmark model is widely used in the emergency evaluation of earthquake-indcued landslides, this method is affected by input parameters and model simplification, resulting in the problem of practicability in the emergency rescue stages (Ma and Xu, 2019b). In recent years, the near real-time coseismic landslide models based on global landslide data have been proposed and tested in some earthquake cases. Allstadt et al. (2018) compare three global earthquake-induced landslide models and use the 2016 Mw 7.8 Kaikoura, New Zealand earthquake to evaluate the performance of three models. The seismic landslide hazard assessment map of this earthquake event is created by the above models and the ShakeMap published by USGS, demonstrating the remarkable potential of the near real-time model in earthquake landslide emergency assessment. Similarly, Xu et al. (2019) establish a new generation of Chinese earthquake-triggered landslide hazard model based on 9 real earthquake-triggered landslide cases. We apply this model to the six earthquake events in the Sichuan Yunnan region and the result shows that although the prediction result based on this model is the landslide hazard estimate with 100m resolution, the model can quickly determine the high-hazard area after the earthquake. Furthermore, with the exception of the Minxian earthquake, the model shows strong prediction ability in other five events, and the AUC values are greater than 0.8 (Fig.11). However, the AUC value of the Minxian event is only 0.57, illustrating that the model is inapplicable in the Minxian region (Fig.11).

The main lithology of the landslides triggered by the earthquake in Minxian region is Pleistocene loess, and thus the main landslide type is small- and medium-sized loess landslide (Xu et al., 2014a). In contrast, the coseismic landslides triggered by other five events are primarily rock landslides. Furthermore, the landform of the Minxian area is typical loess landform with thick loess covering the hillside. The remaining five earthquake zones are typical mountainous landforms with high altitudes and steep slopes, and the rock joints are well developed due to the strong influence of tectonic activity. Therefore, the Minxian earthquake has extremely different geological, topographic, and geomorphic conditions, compared with other five earthquake events. Such differences lead to the poor evaluation ability of the model for the Minxian earthquake. Otherwise, the AUC value of the Wenchuan earthquake is the highest, reaching 0.947 (Fig.11). The Chinese earthquake-triggered landslide hazard model includes more than 300000 real landslide records, of which the landslide records of the Wenchuan earthquake account for more than 60% of the total records. Because of the relative large number of landslides triggered by the Wenchuan event, the global data set remains dominated by this earthquake. The construction of the LR model is most affected by the landslide samples of the Wenchuan events, which leads to the highest applicability and accuracy of the model in the Wenchuan region. The same phenomenon can also be found in previous studies (Nowicki Jessee et al., 2018; Nowicki et al., 2014).

In the first stage, we have to admit that the evaluation results of six earthquakes based on the Xu_{2019} model has yet to be improved. It is prominent that landslide observations from the earthquake match well with the predicted high probabilities, but the model predicts potential landslides in a large area beyond the mapped landslide area. Especially in Minxian, Jiuzhaigou and Yushu earthquake cases, the performance of the model is not satisfactory (Fig.4). Most of the current near-real-time models have such problems that the model performs well when evaluated over the domain of an entire event area, but clearly, individual pixels will predict probabilities that underestimate or overestimate the landslide hazard (Nowicki Jessee et al., 2018). We propose two possible reasons for this phenomenon: (1) The resolution of the input data of the Xu_{2019} model is 100m, which affects the prediction accuracy of the model to a certain extent. Therefore, there may be errors between the modeling prediction and the actual result at the regional scale. (2) Nine earthquake cases used for the establishment of the Xu_{2019} model are located in China and its adjacent areas. The corresponding epicentral areas have different topographic and geological conditions, and only four cases are in the Sichuan-Yunnan area, which may weaken the applicability of the Xu_{2019} model in other quake events. Therefore, in the past few years, we have been constantly supplementing the earthquake landslide database in Sichuan Yunnan region (e.g. 2014 Ms 6.6 Jinggu earthquake, 2020 Ms 5.0 Qiaojia earthquake, 2018 Ms 5.7 Xingwen earthquake, 2019 Ms 6.0 Changning earthquake, 2022 Ms 6.8 Luding earthquake,.etc). We suggest that with the accumulation of enough coseismic landslide inventories in Sichuan-Yunnan area, we can constantly update the near-real-time earthquake-triggered landslide hazard model based on these abundant landslide data and high resolution input factor data, and further improve the accuracy of the modelling in the emergency assessment.

Despite the fact that remote sensing and GIS technology have advanced significantly in recent years, a considerable amount of post-earthquake images may appear within a few hours or days after the earthquake. However, due to the broad quake-affected area, cloud coverage, satellite scheduling and other factors, it is difficult to acquire the post-quake optical imagery immediately (Kargel et al., 2016;

Roback et al., 2018). Therefore, in the temporary resettlement stage II, we can only obtain the images of the meizoseismal area, and carry out visual interpretation or automatic identification of the seismic landslides in this area. Robinson et al. (2017) use the coseismic landslide database of the 2016 Nepal earthquake to conduct the rapid post-earthquake modelling of coseismic landslides. The evaluation results obtained by randomly selecting a small number of landslide samples are not much different from those obtained based on the complete landslide database, indicating that incomplete landslide samples can also be used to conduct seismic landslide hazard assessments. Our findings also reveal that the AUC values of all seismic events in the second stage are greater than 0.8, demonstrating that the prediction results based on incomplete landslide data in the meizoseismal area can better predict the location of the landslides in the entire earthquake area (Fig.11 and 12). Although the Ap calculated by incomplete landslide data is slightly less than the Ao triggered by earthquake events (Fig.10), the prediction model generally has certain applicability in the mid-term stage of the earthquakes, which can better take into account the timeliness and accuracy and thus more effectively serve the post-disaster resettlement in earthquake stricken areas (Ma et al., 2020).

6 Conclusion

The aim of this study is to propose an improved three-stage spatial prediction strategy and evaluate its applicability in six earthquake events. The results reveal that in the first stage, the AUC value of the modelling performance of the Wenchuan earthquake is the highest, reaching 0.947, while the AUC value of the Minxian earthquake is the lowest, only 0.57. In the second and third stages, we can observe that as landslide data is continuously improved, the prediction ability of the model based on the entire landslide database is gradually enhanced. Based on the entire landslide database, the AUC values of six events exceed 0.9, indicating a very high prediction accuracy. Furthermore, the Ap for the six earthquake events in different evaluation stages shows that based on incomplete landslide data in the meizoseismal area, Ap is much smaller than Ao. Nevertheless, when the prediction model based on complete landslide data is built, Ap is nearly identical to Ao. Overall, the prediction results in the first stage can meet the requirements of emergency rescue with quickly obtaining the overall predicted information of the possible coseismic landslide locations in the quake-affected area. With the improvement of the coseismic landslide data in the second and third stages, the accuracy of the prediction results can be more accurate, and thus it can meet the requirement of temporary restoration and later reconstruction. This improved three-stage spatial prediction strategy has preferable practicability for regional landslide prevention and mitigation of major earthquakes in the Sichuan and Yunnan regions.

Author contributions

C.X. conceptualized the work, designed the overall methodology. X.S. wrote the codes of Mat.LShazard and original draft of the paper. S.M. designed the framework of this research, processed the relevant data and performed the overall Mat.LShazard code validation. S.M. and C.X. contributed to the review, editing, and writing of the paper.

Code availability

Mat.LShazard V1.0 is composed of three modules including Data input, model training, and model validation coded as separate matlab script files and can be executed under WindowsOS with the version of MATLAB 2016 or higher. Mat.LShazard V1.0 is free software, and the codes are all public. The code can be available from the corresponding author upon request.

Data availability

Data used in this study include mapped landslide inventories of the 2008 Mw 7.9 Wenchuan earthquake (Xu et al., 2014b), the 2014 Mw 6.6 Ludian earthquake (Wu et al., 2020), the 2013 Mw 6.6 Lushan earthquake (Xu et al., 2015), the 2017 Mw 6.5 Jiuzhaigou earthquake (Tian et al., 2019), the 2013 Mw 5.9 Minxian earthquake (Tian et al., 2016), the 2010 Mw 6.9 Yushu earthquake (Xu and Xu, 2014). A subset of these landslide inventories is publicly available in an open access data repository from https://www.sciencebase.gov/catalog/item/586d824ce4b0f5ce109fc9a6. The elevation data is from 30m resolution SRTM DEM (Jarvis et al., 2008). The distribution of seismic intensity for every seismic event is provided by China Earthquake Networks Center (https://www.cenc.ac.cn/cenc/zgdztw/index.html). Lithology data are from China Geological Survey (http://dcc.cgs.gov.cn/).

Acknowledgments

This study was supported by the National Institute of Natural Hazards, Ministry of Emergency Management of China (ZDJ2021-14) and the Lhasa National Geophysical Observation and Research Station (NORSLS20-07). The authors thank Ali P. Yunus and another anonymous reviewers for their constructive suggestion, which are of great significance to improve the quality of this paper.

References

Allstadt, K.E., Jibson, R.W., Thompson, E.M., Massey, C.I., Wald, D.J., Godt, J.W., Rengers, F.K., 2018. Improving Near‐Real‐Time Coseismic Landslide Models: Lessons Learned from the 2016 Kaikōura, New Zealand, Earthquake. Bulletin of the Seismological Society of America, 108 (3B), 1649-1664.

Bai, S.B., Lu, P., Wang, J., 2015. Landslide susceptibility assessment of the Youfang Catchment using logistic regression. Journal of Mountain Science(04), 816-827.

Bragagnolo, L., da Silva, R.V., Grzybowski, J.M.V., 2020. Landslide susceptibility mapping with r.landslide: A free open-source GIS-integrated tool based on Artificial Neural Networks. Environmental Modelling & Software, 123, 104565.

Brenning, A., 2005. Spatial prediction models for landslide hazards: review, comparison and evaluation. Natural Hazards & Earth System Sciences, 5 (6), 853-862.

Broeckx, J., Vanmaercke, M., Duchateau, R., Poesen, J., 2018. A data-based landslide susceptibility map of Africa. Earth-Science Reviews, 185, 102-121.

Cao, J., Zhang, Z., Wang, C., Liu, J., Zhang, L., 2019. Susceptibility assessment of landslides triggered by earthquakes in the Western Sichuan Plateau. CATENA, 175, 63-76.

Chen, L., Wang, H., Ran, Y., Sun, X., Su, G., Wang, J., Tan, X., Li, Z., Zhang, X., 2010. The MS7.1 Yushu earthquake surface rupture and large historical earthquakes on the Garzê-Yushu Fault. Chinese Science Bulletin, 55 (31), 3504-3509.

Cheng, J., Xu, X., Chen, G., 2020. A new prediction model of seismic hazard for the Sichuan-Yunnan region based on the occurrence rate of large earthquakes. Journal of Geophysics, 63 (3).

Cui, P., Zhu, Y.-y., Han, Y.-s., Chen, X.-q., Zhuang, J.-q., 2009. The 12 May Wenchuan earthquake-induced landslide lakes: distribution and preliminary risk evaluation. Landslides, 6 (3), 209-223.

Dai, F., Lee, C.F., Li, J., Xu, Z.W., 2001. Assessment of landslide susceptibility on the natural terrain of Lantau Island, Hong Kong. Environmental Geology, 40 (3), 381-391.

Dai, F.C., Lee, C.F., 2002. Landslide characteristics and slope instability modeling using GIS, Lantau Island, Hong Kong. Geomorphology, 42 (3), 213-228.

Demir, G., Aytekin, M., Akgün, A., İkizler, S.B., Tatar, O., 2013. A comparison of landslide susceptibility mapping of the eastern part of the North Anatolian Fault Zone (Turkey) by likelihood-frequency ratio and analytic hierarchy process methods. Natural Hazards, 65 (3), 1481-1506.

Dreyfus, D.K., Rathje, E.M., Jibson, R.W., 2013. The influence of different simplified sliding-block models and input parameters on regional predictions of seismic landslides triggered by the Northridge earthquake. Engineering Geology, 163, 41-54.

Ercanoglu, M., Temiz, F.A., 2011. Application of logistic regression and fuzzy operators to landslide susceptibility assessment in Azdavay (Kastamonu, Turkey). Environmental Earth Sciences, 64 (4), 949-964.

Fawcett, T., 2006. An introduction to ROC analysis. Pattern Recognition Letters, 27 (8), 861-874.

Fick, S.E., Hijmans, R.J., 2017. WorldClim 2: new 1-km spatial resolution climate surfaces for global land areas. International Journal of Climatology, 37 (12), 4302-4315.

Guzzetti, F., Paola, R., Cardinali, M., Galli, M., Ardizzone, F., 2005. Probablistic landslide hazard assessment at the basin scale. Geomorphology, 72, 272-299.

He, Q., Wang, M., Liu, K., 2021. Rapidly assessing earthquake-induced landslide susceptibility on a global scale using random forest. Geomorphology, 391, 107889.

Huang, R., Fan, X., 2013. The landslide story. Nature Geoscience, 6 (5), 325-326.

Jarvis, A., Reuter, H., Nelson, A., Guevara, E., 2008. Hole-filled seamless SRTM data v4. International Centre for Tropical Agriculture (CIAT).

Jenness, J., Brost, B., Beier, P., 2013. Land facet corridor designer: Topographic position index. www.jennessent.com.

Jiang, W., Zhang, J., Tian, T., Wang, X., 2012. Crustal structure of Chuan-Dian region derived from gravity data and its tectonic implications. Physics of the Earth and Planetary Interiors, 212-213, 76-87.

Jibson, R.W., Harp, E.L., Michael, J.A., 2000. A method for producing digital probabilistic seismic landslide hazard maps: An example from the Los Angeles, California, area. Engineering Geology, 58 (3–4), 271-289.

Kargel, J.S., Leonard, G.J., Shugar, D.H., Haritashya, U.K., Bevington, A., Fielding, E.J., Fujita, K., Geertsema, M., Miles, E.S., Steiner, J., Anderson, E., Bajracharya, S., Bawden, G.W., Breashears, D.F., Byers, A., Collins, B., Dhital, M.R., Donnellan, A., Evans, T.L., Geai, M.L., Glasscoe, M.T., Green, D., Gurung, D.R., Heijenk, R., Hilborn, A., Hudnut, K., Huyck, C., Immerzeel, W.W., Liming, J., Jibson, R., Kääb, A., Khanal, N.R., Kirschbaum, D., Kraaijenbrink, P.D.A., Lamsal, D., Shiyin, L., Mingyang, L., McKinney, D., Nahirnick, N.K., Zhuotong, N., Ojha, S., Olsenholler, J., Painter, T.H., Pleasants, M., Pratima, K.C., Yuan, Q.I., Raup, B.H., Regmi, D., Rounce, D.R., Sakai, A., Donghui, S., Shea, J.M., Shrestha, A.B., Shukla, A., Stumm, D., van der Kooij, M., Voss, K., Xin, W., Weihs, B., Wolfe, D., Lizong, W., Xiaojun, Y., Yoder, M.R., Young, N., 2016. Geomorphic and geologic controls of geohazards induced by Nepal's 2015 Gorkha earthquake. Science, 351 (6269), aac8353.

Kritikos, T., Robinson, T.R., Davies, T.R.H., 2015. Regional coseismic landslide hazard assessment without historical landslide inventories: A new approach. Journal of Geophysical Research Earth Surface, 120 (4), 711-729.

Lan, H., Tian, N., Li, L., Liu, H., Peng, J., Cui, P., Zhou, C., Macciotta, R., Clague, J.J., 2022. Poverty control policy may affect the transition of geological disaster risk in China. Humanities and Social Sciences Communications, 9 (1), 80.

Lari, S., Frattini, P., Crosta, G.B., 2014. A probabilistic approach for landslide hazard analysis. Engineering Geology, 182, 3-14.

Lin, L., Lin, Q., Wang, Y., 2017. Landslide susceptibility mapping on a global scale using the method of logistic regression. Nat. Hazards Earth Syst. Sci., 17 (8), 1411-1424.

Liu, J., Wang, T., Shi, J., Li, Z., 2017. Emergency Rapid Assessment of Landslides Induced by the Jiuzhaigou M s 7.0 earthquake, Sichuan, China. Journal of Geomechanics, 23 (5), 639-645.

Ma, S., Xu, C., 2019a. Applicability of Two Newmark Models in the Assessment of Coseismic Landslide Hazard and Estimation of Slope-Failure Probability: An Example of the 2008 Wenchuan Mw 7.9 Earthquake Affected Area. Journal of Earth Science, 30 (5), 1020-1030.

Ma, S., Xu, C., Shao, X., 2020. Spatial prediction strategy for landslides triggered by large earthquakes oriented to emergency response, mid-term resettlement and later reconstruction. International Journal of Disaster Risk Reduction, 43, 101362.

Ma, S.Y., Xu, C., 2019b. Assessment of co-seismic landslide hazard using the Newmark model and statistical analyses: a case study of the 2013 Lushan, China, Mw6.6 earthquake. Natural Hazards, 96 (1), 389-412.

Massey, C., Townsend, D., Rathje, E., Allstadt, K.E., Lukovic, B., Kaneko, Y., Bradley, B., Wartman, J., Jibson, R.W., Petley, D.N., Horspool, N., Hamling, I., Carey, J., Cox, S., Davidson, J., Dellow, S., Godt, J.W., Holden, C., Jones, K., Kaiser, A., Little, M., Lyndsell, B., McColl, S., Morgenstern, R., Rengers, F.K., Rhoades, D., Rosser, B., Strong, D., Singeisen, C., Villeneuve, M., 2018. Landslides Triggered by the 14 November 2016 Mw 7.8 Kaikōura Earthquake, New Zealand. Bulletin of the Seismological Society of America, 108 (3B), 1630-1648.

Merghadi, A., Yunus, A.P., Dou, J., Whiteley, J., ThaiPham, B., Bui, D.T., Avtar, R., Abderrahmane, B., 2020. Machine learning methods for landslide susceptibility studies: A comparative overview of algorithm performance. Earth-Science Reviews, 207, 103225.

Nowicki Jessee, M.A., Hamburger, M.W., Allstadt, K., Wald, D.J., Robeson, S.M., Tanyas, H., Hearne, M., Thompson, E.M., 2018. A global empirical model for near-real-time assessment of seismicallyinduced landslides. Journal of Geophysical Research: Earth Surface, 123 (8), 1835-1859.

Nowicki, M.A., Wald, D.J., Hamburger, M.W., Hearne, M., Thompson, E.M., 2014. Development of a globally applicable model for near real-time prediction of seismically induced landslides. Engineering Geology, 173, 54-65.

Osna, T., Sezer, E.A., Akgun, A., 2014. GeoFIS: An integrated tool for the assessment of landslide susceptibility. Computers & Geosciences, 66, 20-30.

Polat, A., 2021. An innovative, fast method for landslide susceptibility mapping using GIS-based LSAT toolbox. Environmental Earth Sciences, 80 (6), 217.

Pradhan, B., Saro, L., 2010. Landslide susceptibility assessment and factor effect analysis: backpropagation artificial neural networks and their comparison with frequency ratio and bivariate logistic regression modelling. Environmental Modelling & Software, 25 (6), 747-759.

Reichenbach, P., Rossi, M., Malamud, B.D., Mihir, M., Guzzetti, F., 2018. A review of statistically-based landslide susceptibility models. Earth-Science Reviews, 180, 60-91.

Ren, J., Xu, X., Lv, Y., Wang, Q., Li, A., Li, K., Zhu, J., Cai, J., Liu, S., 2022. Late Quaternary slip rate of the northern Lancangjiang fault zone in eastern Tibet: Seismic hazards for the Sichuan-Tibet Railway and regional tectonic implications. Engineering Geology, 106748.

Roback, K., Clark, M.K., West, A.J., Zekkos, D., Li, G., Gallen, S.F., Chamlagain, D., Godt, J.W., 2018. The size, distribution, and mobility of landslides caused by the 2015 Mw7.8 Gorkha earthquake, Nepal. Geomorphology, 301, 121-138.

Robinson, T.R., Rosser, N.J., Densmore, A.L., Williams, J.G., Kincey, M.E., Benjamin, J., Bell, H.J.A., 2017. Rapid post-earthquake modelling of coseismic landslide intensity and distribution for emergency response decision support. Nat. Hazards Earth Syst. Sci., 17 (9), 1521-1540.

Rossi, M., Reichenbach, P., 2016. LAND-SE: a software for statistically based landslide susceptibility zonation, version 1.0. Geoscientific Model Development, 9 (10), 3533-3543.

Shao, X., Ma, S., Xu, C., Xu, X., 2020a. Effects of raster resolution on real probability of landslides. Remote Sensing Applications: Society and Environment, 19, 100364.

Shao, X., Ma, S., Xu, C., Zhou, Q., 2020b. Effects of sampling intensity and non-slide/slide sample ratio on the occurrence probability of coseismic landslides. Geomorphology, 363, 107222.

Shao, X., Xu, C., 2022. Earthquake-induced landslides susceptibility assessment: A review of the state-of-the-art. Natural Hazards Research.

Sun, J., Yue, H., Shen, Z., Fang, L., Zhan, Y., Sun, X., 2018. The 2017 Jiuzhaigou Earthquake: A Complicated Event Occurred in a Young Fault System. Geophysical Research Letters, 45 (5), 2230-2240.

Swets, J.A., 1988. Measuring the accuracy of diagnostic systems. Science, 240 (4857), 1285-1293.

Tanyas, H., Rossi, M., Alvioli, M., van Westen, C.J., Marchesini, I., 2019. A global slope unit-based method for the near real-time prediction of earthquake-induced landslides. Geomorphology, 327, 126-146.

Tapponnier, P., Zhiqin, X., Roger, F., Meyer, B., Arnaud, N., Wittlinger, G., Jingsui, Y., 2001. Oblique stepwise rise and growth of the Tibet plateau. Science, 294 (5547), 1671-1677.

Tateishi, R., 2010. Production of global land cover data-GLCNMO. T. J. Digital Earth, 4, 22-49.

Tian, Y., Owen, L.A., Xu, C., Ma, S., Li, K., Xu, X., Figueiredo, P.M., Kang, W., Guo, P., Wang, S., Liang, X., Maharjan, S.B., 2020. Landslide development within 3 years after the 2015 Mw 7.8 Gorkha earthquake, Nepal. Landslides, 17 (5), 1251-1267.

Tian, Y., Xu, C., Ma, S., Xu, X., Wang, S., Zhang, H., 2019. Inventory and Spatial Distribution of Landslides Triggered by the 8th August 2017 MW 6.5 Jiuzhaigou Earthquake, China. Journal of Earth Science, 30 (1), 206-217.

Tian, Y., Xu, C., Xu, X., Chen, J., 2016. Detailed inventory mapping and spatial analyses to landslides induced by the 2013 Ms 6.6 Minxian earthquake of China. Journal of Earth Science, 27 (6), 1016-1026.

Tolles, J., Meurer, W.J., 2016. Logistic Regression: Relating Patient Characteristics to Outcomes. JAMA, 316 (5), 533-534.

Torizin, J., Schüßler, N., Fuchs, M., 2022. Landslide Susceptibility Assessment Tools v1.0.0b – Project Manager Suite: a new modular toolkit for landslide susceptibility assessment. Geoscientific Model Development, 15 (7), 2791-2812.

Umar, Z., Pradhan, B., Ahmad, A., Jebur, M.N., Tehrany, M.S., 2014. Earthquake induced landslide susceptibility mapping using an integrated ensemble frequency ratio and logistic regression models in West Sumatera Province, Indonesia. Catena, 118, 124-135.

Wang, Y., Song, C., Lin, Q., Li, J., 2016. Occurrence probability assessment of earthquake-triggered landslides with Newmark displacement values and logistic regression: The Wenchuan earthquake, China. Geomorphology, 258, 108-119.

Wu, W., Xu, C., Wang, X., Tian, Y., Deng, F., 2020. Landslides Triggered by the 3 August 2014 Ludian (China) Mw 6.2 Earthquake: An Updated Inventory and Analysis of Their Spatial Distribution. Journal of Earth Science, 31 (4), 853-866.

Xu, C., Dai, F., Xu, X., Yuan, H.L., 2012. GIS-based support vector machine modeling of earthquake-triggered landslide susceptibility in the Jianjiang River watershed, China. Geomorphology, 145-146 (2), 70-80.

Xu, C., Xu, X., 2014. Statistical analysis of landslides caused by the Mw 6.9 Yushu, China, earthquake of April 14, 2010. Natural Hazards, 72 (2), 871-893.

Xu, C., Xu, X., Shyu, J.B.H., 2015. Database and spatial distribution of landslides triggered by the Lushan, China Mw 6.6 earthquake of 20 April 2013. Geomorphology, 248, 77-92.

Xu, C., Xu, X., Shyu, J.B.H., Zheng, W., Min, W., 2014a. Landslides triggered by the 22 July 2013 Minxian–Zhangxian, China, Mw 5.9 earthquake: Inventory compiling and spatial distribution analysis. Journal of Asian Earth Sciences, 92, 125-142.

Xu, C., Xu, X., Yao, X., Dai, F., 2014b. Three (nearly) complete inventories of landslides triggered by the May 12, 2008 Wenchuan Mw 7.9 earthquake of China and their spatial distribution statistical analysis. Landslides, 11 (3), 441-461.

Xu, C., Xu, X., Zheng, W., Wei, Z., Tan, X., Han, Z., Li, C., Liang, M., Li, Z., Wang, H., 2013. landslides triggered by the April 20,2013 Lushan, Sichuan province M_s 7.0 strong erathquake of China. Seismological geology, 35 (3), 641-660.

Xu, C., Xu, X., Zhou, B., Shen, L., 2019. Probability of coseimic landslides: A new generation of earthquake-triggered landslide hazard model. Journal of Engineering Geology, 27 (5), 1122.

Xu, X., Han, Z., Yang, X., 2016. Seismotectonic map in China and its adjacent regions. Seismological Press, Beijing.

Xu, X., Zhang, P., Wen, X., Qin, Z., Chen, G., Zhu, A., 2005. Features of active tectonics and recurrence behaviors of strong earthquakes in the western Sichuan province and its adjacent regions. Sesimology and geology, 27 (3), 446.

Xu, X.W., Wen, X.Z., Yu, G.H., Chen, G.H., Klinger, Y., Hubbard, J., Shaw, J., 2009. Coseismic reverse- and oblique-slip surface faulting generated by the 2008 Mw 7.9 Wenchuan earthquake, China. Geology, 37 (6), 515-518.

Yao, X., Tham, L.G., Dai, F.C., 2008. Landslide susceptibility mapping based on Support Vector Machine: A case study on natural slopes of Hong Kong, China. Geomorphology, 101 (4), 572-582.

Zhang, P., Deng, Q., Zhang, G., Ma, J., Gan, W., Min, W., Mao, F., Wang, Q., 2003. Active tectonic blocks and strong earthquakes in the continent of China. Science in China Series D: Earth Sciences, 46 (2), 13-24.

Zhao, B., Zhao, X., Zeng, L., Wang, S., Du, Y., 2021. The mechanisms of complex morphological features of a prehistorical landslide on the eastern margin of the Qinghai-Tibetan Plateau. Bulletin of Engineering Geology and the Environment, 80 (4), 3423-3437.

Zheng, W., Yuan, D., He, W., Min, W., Ren, Z., Liu, X., Wang, A., Xu, C., Ge, W., Li, F., 2013. Geometric pattern and active tectonics in Southeastern Gansu province: Discussion on seismogenic mechanism of the Minxian-Zhangxian M(S)6. 6 earthquake on July 22, 2013. Chinese Journal

of Geophysics, 56 (12), 4058-4071.
Zhuang, J., Peng, J., Zhu, X., Huang, W., 2019. Scenario-Based Risk Assessment of Earthquake Disaster Using Slope Displacement, PGA, and Population Density in the Guyuan Region, China. ISPRS International Journal of Geo-Information, 8 (2), 85.